Molecular Crystals and Liquid Crystals
Publication details, including instructions for authors and subscription information:
http://www.tandfonline.com/loi/gmcl20

A Highly Accurate Measurement of Liquid Crystal Material and Device Parameters

Takahiro Ishinabe [a] & Tatsuo Uchida [a]
[a] Department of Electronics, Graduate School of Engineering, Tohoku University, Aramaki, Aoba-ku, Sendai, Japan

Version of record first published: 22 Feb 2010

To cite this article: Takahiro Ishinabe & Tatsuo Uchida (2010): A Highly Accurate Measurement of Liquid Crystal Material and Device Parameters, Molecular Crystals and Liquid Crystals, 516:1, 211-227

To link to this article: http://dx.doi.org/10.1080/15421400903409374

Mol. Cryst. Liq. Cryst., Vol. 516: pp. 211–227, 2010

ISSN: 1542-1406 print/1563-5287 online
DOI: 10.1080/15421400903409374

Taylor & Francis
Taylor & Francis Group

A Highly Accurate Measurement of Liquid Crystal Material and Device Parameters

TAKAHIRO ISHINABE AND TATSUO UCHIDA

Department of Electronics, Graduate School of Engineering, Tohoku University, Aramaki, Aoba-ku, Sendai, Japan

A highly accurate measurement method for the refractive indices of liquid crystal materials, the alignment distribution and the surface polar anchoring strength was devised by considering the multiple reflections and the interferences in the LC cell. Based on the accurate evaluation of LC devices, we developed the high-quality field sequential color liquid crystal display with a wide viewing angle and high contrast ratio.

Keywords Alignment distribution; field sequential color LCD; liquid crystal; OCB-mode; polar anchoring strength; refractive indices

1. Introduction

With improvements in quality and performance, the liquid crystal display (LCD) has spread into a wide variety of applications, including personal computers, cellular phones and televisions. Since the LCDs use the optical anisotropy of LC, its optical performance depends on the refractive indices, the alignment distribution of LC, and the thickness of the LC cell. With the recent advances in the viewing angle and the contrast ratio of LCDs, it has become important to measure these parameters with high accuracy. In addition, the evaluation of the surface anchoring strength also has become important in the optical design of liquid crystal displays because it controls the alignment distribution of LCs.

On the other hand, optically compensated bend (OCB) mode [1] is a promising technology as the future high quality display devices due to its wide viewing angle without gray scale inversion and color shift, fast response speed, high contrast ratio in both still and moving images, and wide temperature range [2]. For the purpose of improving the optical performance of OCB-mode LCD, it is necessary to compensate the viewing angle dependence of bend-alignment LC cell, and the optical compensation using the polymerized discotic material (PDM) compensation film has been considered as one of the most effective method to improve the optical performance of OCB-mode LCD [3,4]. The PDM compensation film is composed of a biaxial film substrate and a PDM-layer. However, it was difficult to accurately evaluate the

Address correspondence to Takahiro Ishinabe, Department of Electronics, Graduate School of Engineering, Tohoku University, 6-6-05 Aoba, Aramaki, Aoba-ku, Sendai 980-8579, Japan. E-mail: ishinabe@ecei.tohoku.ac.jp

alignment distribution of the PDM-layer, and thus the optical optimization of the OCB mode LC-cell has depended mainly on try and error. As a result, there is still room for improvement in terms of the contrast ratio and the viewing angle of the OCB mode, compared with the in-plane switching (IPS) and vertically aligned (VA) modes.

In the present work, we aimed to realize a high-precision measurement of the refractive indices of LC materials, the cell thickness, the alignment distribution of LC, and the polar anchoring strength. In addition, we discuss the evaluation of the PDM compensation film and the development of the OCB mode LCD with high contrast ratio and wide viewing angle range based on the highly accurate measurement methods.

2. Measurement of the Refractive Indices of LC Material and the Cell Thickness

2.1. *A Highly Accurate Method for Measuring the Refractive Indices*

In general, the LC cell thickness is obtained from a measurement of the phase retardation of LC cell and the refractive indices of LC materials, and therefore the measurement accuracy of the cell thickness depends on that of the refractive indices. The refractive indices of LC materials have been measured by an Abbe refractometer, however this method has a problem in accuracy because it is difficult to control the alignment distribution of a LC homogeneously. As a result, measurement accuracy decreases also in the measurement of the LC cell thickness. In this section, we aimed to establish a highly accurate measurement procedure for the ordinary and extraordinary refractive indices of LC materials and the cell thickness.

A measurement method for the refractive indices using multiple interferences in the LC cell has been previously proposed [5,6]. In this method, an alignment layer material of polyvinyl alcohol which has a refractive index near that of glass substrate is used, and the wavelength dependences of the amplitude ratio Ψ and phase difference Δ (or phase retardation δ) at the normal incidence are measured and the refractive indices of LC material were determined from the numerical fitting between the measured and theoretical values by considering the multiple reflections and the multiple interferences in the LC cell.

However, we found that this method has multiple solutions in the combination of the refractive indices and the cell thickness and it is difficult to obtain the correct value of the refractive indices. As an example, Figure 1 shows the calculated result of an optical characteristic at the normal incidence for two LCs: LC1 and LC2 that have the refractive index shown in Figure 2. In this figure, the optical characteristics of both LCs are almost identical in the wavelength dependences of Ψ and δ (or Δ), and therefore it is found that the only solution of the refractive indices and the cell thickness cannot be obtained from this fitting method. The measure result of refractive indices for several LC-cells with different cell gaps is shown in Figure 3.

The ordinary and the extraordinary refractive indices changed according to LC cell thicknesses and we confirmed that accurate values cannot be obtained by the conventional multiple interferences method using normal incidence.

In this study, we found that this problem can be solved by using the phase retardation characteristic at oblique incidences. Figure 4 shows the calculated result of the $\lambda-\delta$ characteristics at an oblique incidence of the two LCs: LC1 and LC2.

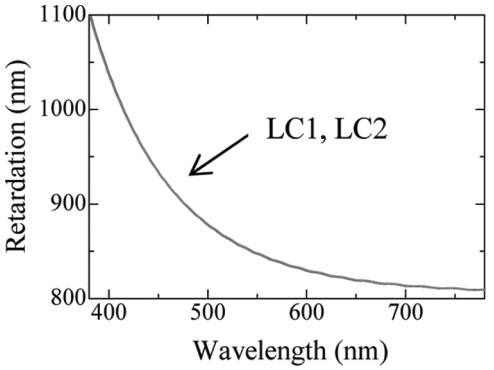

Figure 1. Wavelength-Phase retardation characteristics of the LC-cell 1 and 2 at normal incidence.

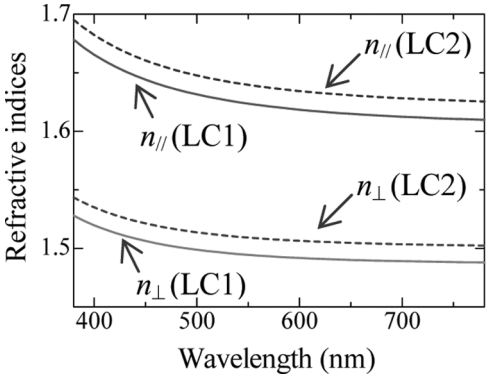

Figure 2. Refractive indices of the LC 1 and 2.

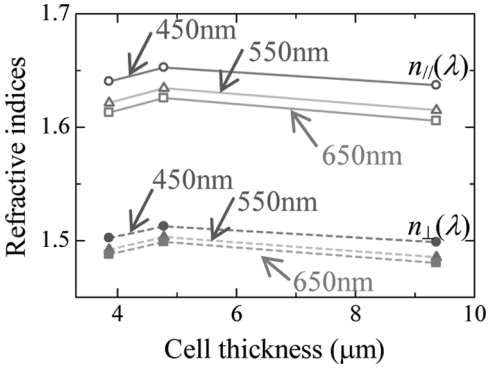

Figure 3. Measured results of $n_{\perp}$ (λ) and $n_{//}$ (λ) of various cell thicknesses using the conventional method.

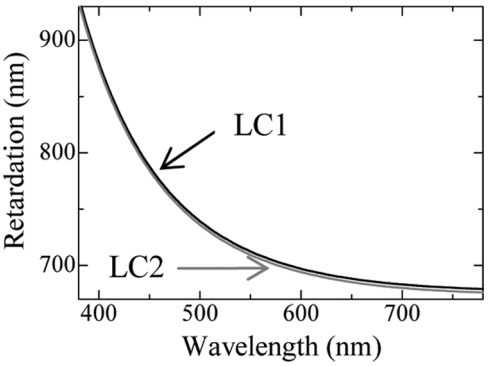

Figure 4. Calculated result of phase retardation characteristics at oblique incidence.

We found that $\lambda-\delta$ characteristics are not corresponding in the oblique incidence even if these LCs have the same property in the normal incidence as shown in Figure 1.

As a result, we clarified that the refractive indices and the LC cell thickness can be measured with high accuracy by the following procedure. The homogeneous cell is made by using the alignment layer material that has a refractive index greatly different from that of the glass substrate. The wavelength dependences of the amplitude ratio and the phase retardation at normal and oblique incidences are measured. The refractive indices and the LC cell thickness are decided from the numerical fitting between the measured values and the theoretical values in which the multiple reflections and the multiple interferences in the liquid crystal cell are considered. To accomplish this measurement method, theoretical values must be calculated considering the multiple reflections and the multiple interferences in the multilayer media. Therefore, we extended the Jones matrix method to consider the multiple reflections and the multiple interferences.

2.2. *New Extended Jones Matrix Method Considering the Multiple Interferences*

In the conventional Jones matrix method [7,8], the transmitted light Jones vector (A_{pout}, A_{sout}) is calculated by multiplying the Jones matrix $\mathbf{X}_i$ of the media by the incident light Jones vector (A_{pin}, A_{sin}), as follows:

$$\begin{bmatrix} A_{\mathrm{pout}} \\ A_{\mathrm{sout}} \end{bmatrix} = \mathbf{X}_i \begin{bmatrix} A_{\mathrm{pin}} \\ A_{\mathrm{sin}} \end{bmatrix}. \tag{1}$$

The Jones matrix $\mathbf{X}_1$ of one layer of the medium is derived from Eq. (2):

$$\mathbf{X}_1 = \mathbf{T}_{1,2}\mathbf{\Phi}_1\Gamma_1\mathbf{\Phi}_1^{-1}\mathbf{T}_{0,1}, \tag{2},$$

where $\mathbf{T}_{\mathrm{i,j}}$ is the transmittance matrix between layers i and j, $\mathbf{\Phi}_{\mathrm{i}}$ is the transformation matrix of layer i, and $\mathbf{\Gamma}_{\mathrm{i}}$ is the propagation matrix. In general, the Jones matrix method does not consider the multiple reflections and the multiple interferences. As shown in Eq. (3), however a Jones matrix that includes the multiple reflections and the multiple interferences for one layer of medium can be derived by defining

the interference matrix $\mathbf{G}_1$ and calculating the superposition of transmitted light, including that transmitted after it reflects within the layer:

$$\mathbf{X}_1 = \mathbf{T}_{1,2}(\mathbf{E} + \mathbf{G}_1 + \mathbf{G}_1^2 + \mathrm{L})\mathbf{A}_1\mathbf{T}_{0,1}, \quad \mathbf{G}_1 = \mathbf{M}_1\mathbf{R}_{1,0}\mathbf{M}_1\mathbf{R}_{1,2}, \quad \mathbf{M}_1 = \mathbf{\Phi}_1\Gamma_1\mathbf{\Phi}_1^{-1}, \quad (3)$$

where $\mathbf{R}_{i,j}$ is the reflection matrix between layers *i* and *j*. A Jones matrix that considers the multiple reflections and the multiple interferences of *N* layers of media can be derived by extending Eq. (3) to *N* layers of media and calculating the transmitted and the reflected light between all layers. We confirmed that the good agreement was obtained on comparing this technique to the 4×4 matrix method [9], and a Jones matrix method that considers the multiple reflections and the multiple interferences for calculations involving multilayer media was established.

2.3. *Measurement of the Refractive Indices of LC Materials*

We measured the refractive indices by using the procedure devised in this study. We used SE7992 (Nissan Chemical Industry) as an alignment layer material. First, we measured the thickness, refractive index, and absorption coefficient of the glass substrate and the alignment layer material by using our new Extended Jones Matrix Method. Next, we made a LC cell using the LC material of TD1016XX (Chisso), and then the wavelength dependence of the amplitude ratio and the phase retardation at normal and oblique incident angles were measured by an Ellipsometer M-2000 (J. A. Woollam). We determined the refractive indices and the LC cell thickness by the numerical fitting between the measurements and theoretical values considering the multiple reflections and the multiple interferences. The fitting results and derived refractive indices are shown in Figures 5 and 6, respectively. The measurements were found to correspond well to the calculated values for all angles of incidences, as shown in the figure.

To confirm the validity of this procedure, LC cells of various thicknesses were made and the refractive indices were measured. The results are shown in Figure 7.

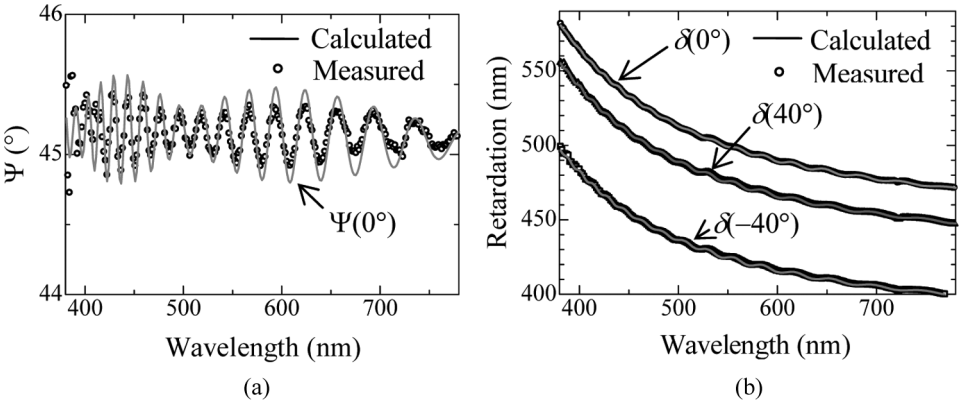

Figure 5. Fitting results in the amplitude ratio and the phase retardation properties. (a) Fitting result of the wavelength - amplitude ratios Ψ dependences; (b) Fitting results of the wavelength - phase retardation δ dependences.

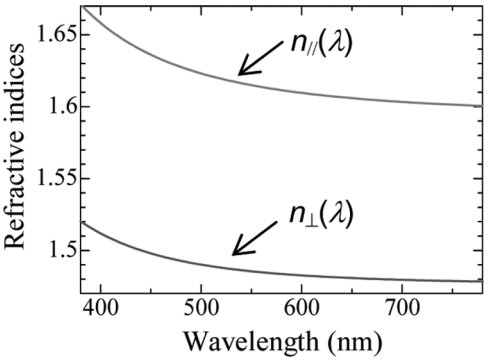

Figure 6. Measure result of refractive indices.

The refractive indices were shown to be constant with respect to cell thickness, thereby confirming the validity of the new method.

3. Measurement of Alignment Distribution and Anchoring Strength of LC

3.1. *Problems of the Conventional Measurement Method*

Recently, several measurement methods for the alignment distribution and the polar anchoring strength of LC have been proposed [10–17]. However, we found that these methods have problems such as a difficulty of the high precision measurement, a difficulty of the evaluation of the vertical alignment layer or a complication of the measurement system. In addition, there has been little discussion on a validity of the measure result of these methods, it is also a problem. Therefore, the establishment of a simple and highly accurate measurement method for the alignment distribution and the polar anchoring strength has become an important problem.

As a simple measurement method for the anchoring strength of parallel and vertical alignment layer, Hung and the present authors proposed a method which used the hybrid alignment nematic (HAN) liquid crystal cells [11–13]. In these methods, the angular dependence of phase retardation was measured in the direction parallel to the alignment plane of the HAN cell, and the polar anchoring strengths was

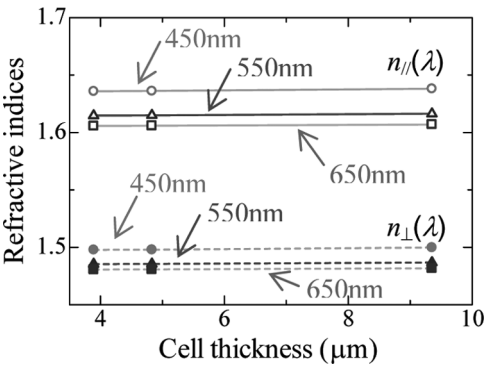

Figure 7. Experimental results of the refractive indices for several cell thicknesses.

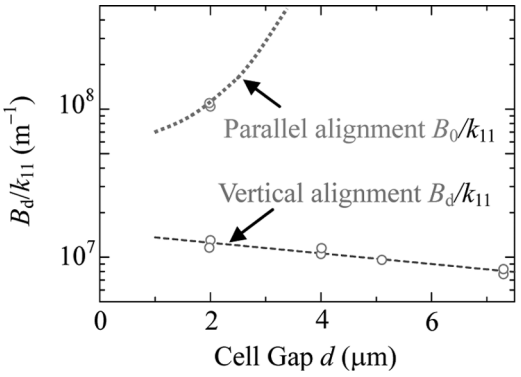

Figure 8. Measured result of the polar anchoring strength by the conventional method.

calculated by determining the cell thickness and the pre-tilt angles of the parallel and vertically aligned layers through the numerical fitting between the measured and the theoretical values. Here, the elastic constant ratio κ was previously measured and treated as the known parameter in these methods.

However, we found that the value of the polar anchoring strength obtained by these methods highly depends on a measurement accuracy of the elastic constant ratio κ, because the error of the elastic constant ratio κ causes the measurement error of the alignment distribution of HAN cell. In order to confirm the validity of the conventional method, we measured the polar anchoring strength using LC-cells with different cell thickness. Figure 8 shows the measured result of cell gap dependence of polar anchoring strength measured by the conventional method. It is seen from this figure that the obtained polar anchoring strength has cell gap dependence due to a low accuracy of the elastic constant ratio κ. Therefore, this method suffers from the problem of difficulty in measuring the polar anchoring strength with a high degree of precision. As a result, we found that the elastic constant ratio κ must be measured in this fitting method as well as the pretilt angle θ_0, θ_d and the cell thickness d to realize a high-precision measurement for the polar anchoring strength.

In this section, we aimed to realize a high-precision measurement of the cell thickness, the elastic constant ratio, and the polar anchoring strength based on the investigation of the relation between the angular optical characteristics and the alignment distribution of HAN cell.

3.2. *Analysis of the Problems Inherent in the Previous Measurement Methods*

In a hybrid alignment cell, the tilt angle from the interface of the parallel alignment layer to the interface of the vertical alignment layer is distributed in such a way as to satisfy Eq. (4).

$$(1 + \kappa \sin^2 \theta)(d\theta/dz)^2 = C^2 \tag{4}$$

where θ denotes the tilt angle for the liquid crystal molecule, C is the integration constant, and κ is a quantity defined by Eq. (5).

$$\kappa = \frac{k_{33}}{k_{11} - 1} \tag{5}$$

where k_{11} and k_{33} are splay and bend elastic constants, respectively. Cell thickness d, tilt angle θ_0 on the horizontal alignment layer side, and tilt angle θ_d on the vertical alignment layer side are determined by numerical fitting of the measurement data with respect to the theoretical values. Using these values, the polar anchoring strengths B_0 and B_d on the parallel and vertical alignment layer sides can be determined from Eqs. (6) and (7), respectively.

$$\frac{B_d}{k_{11}} = \frac{\sqrt{1 + \kappa \sin^2 \theta_d}}{\sin 2\theta_d} C \tag{6}$$

$$\frac{B_0}{k_{11}} = \frac{\sqrt{1 + \kappa \sin^2(\theta_0 - \theta_e)}}{\sin 2(\theta_0 - \theta_e)} C \tag{7}$$

where θ_e denotes the alignment easy axis direction of the parallel alignment layer [18].

We examined the application of this fitting method to the measurement of the elastic constant ratio κ. We investigated the influence of the elastic constant ratio κ, cell thickness d, and pretilt angles θ_0 and θ_d toward the incident angle dependence of phase retardation of HAN call. As a result, we found that the multiple combinations of d, κ, θ_0 and θ_d which have the same phase retardation angle characteristics exist. This result is explained as follows. In the direction parallel to the alignment plane, the direction of the optical axis of the liquid crystal director becomes uniform. As a result, the propagation of light becomes the Eigen-mode and the multiple combinations of alignment distribution have the same incident angle dependence of phase retardation.

For example, we have derived the combination of the d, κ, θ_0 and θ_d having the phase retardation angle characteristics same as the liquid crystal alignment calculated by using the parameters listed in Table 1. Table 2 shows the example of the results of the derivation of alignment distribution. Similarly, Figure 9 shows the angular characteristics of the phase retardation of the LC cell listed in Table 2. This figure shows that the respective phase retardation angle characteristics become identical by choosing appropriate values of θ_0 and θ_d for a given κ. These results show that the elastic constant ratio κ cannot be obtained by this fitting method as well as the d, θ_0 and θ_d and this approach has a problem of low accuracy in the measurement of the polar anchoring strength.

3.3. *Proposal of the New Measurement Method with High Accuracy*

This problem can be solved by introducing a twist distribution in the direction of the optical axis of LC director and by shifting the propagation of light from the

Table 1. Alignment parameters of original HAN cell

d	5 μm
θ_0	2°
θ_d	88°
κ	−0.15146
n_e	1.6664
n_o	1.5075

Table 2. Values of d, κ, θ_0 and θ_d which have the same phase retardation angle characteristics with that of Table 1

κ	θ_0 (°)	θ_d (°)	d (μm)
1	−2.39	83.59	5.00
0.5	−0.80	84.96	5.00
0	1.24	87.08	5.00
−0.15	1.99	87.99	5.00
−0.5	4.22	91.26	5.00

Eigen-mode. Generally, the distribution of the optical axis of the liquid crystal has twist distribution with respect to the incident rays in the direction perpendicular to the rubbing direction of the HAN cell as shown in Figure 10. Consequently, it is conceivable that the d, κ, θ_0, and θ_d can be derived with high precision by measuring the angular characteristics in the direction perpendicular to the alignment plane as shown Figure 11. In view of the fact that the alignment distribution of the liquid crystal in the perpendicular direction has a twist distribution, it is not possible to measure the phase retardation of the liquid crystal cell. Therefore, we studied the parameters to be measured in the perpendicular direction. As a result, for the analysis of characteristics in the direction perpendicular to the alignment plane of LCs, we found that the amplitude ratios Ψ_{AnE}, Ψ_{Aps}, and Ψ_{Asp} and the phase differences Δ_{AnE}, Δ_{Aps}, and Δ_{Asp} must be employed due to the effective twist of LCs. The amplitude ratios and the phase differences are defined as

$$\tan \Psi_{\mathrm{AnE}} e^{i\Delta_{\mathrm{AnE}}} = \frac{\rho_{\mathrm{pp}}}{\rho_{\mathrm{ss}}}, \tag{7a}$$

$$\tan \Psi_{\mathrm{Aps}} e^{i\Delta_{\mathrm{Aps}}} = \frac{\rho_{\mathrm{ps}}}{\rho_{\mathrm{pp}}}, \tag{7b}$$

$$\tan \Psi_{\mathrm{Asp}} e^{i\Delta_{\mathrm{Asp}}} = \frac{\rho_{\mathrm{sp}}}{\rho_{\mathrm{ss}}}, \tag{7c}$$

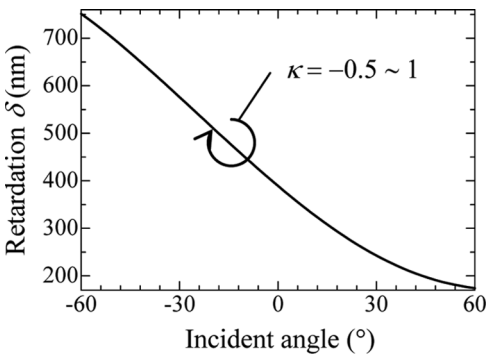

Figure 9. Incident angle dependence of phase retardation of the HAN cell listed in Table 2.

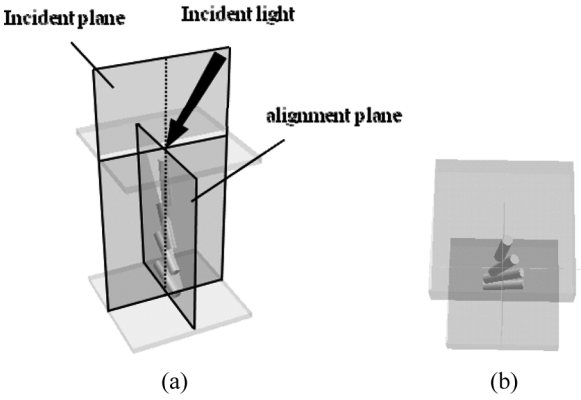

Figure 10. Twist distribution in the direction perpendicular to the alignment plane of HAN cell. (a) The case which incident light enters into HAN cell from perpendicular azimuth direction to the alignment plane; (b) Alignment distribution of HAN cell seen from the incident light.

where ρ_{pp}, ρ_{ss}, ρ_{ps}, and ρ_{sp} are elements of the Jones matrix **M** of a HAN cell, and **M** is shown as

$$\mathbf{M} = \begin{pmatrix} \rho_{pp} & \rho_{sp} \\ \rho_{ps} & \rho_{ss} \end{pmatrix} \tag{8}$$

M is calculated by the extended Jones matrix method as follows,

$$\mathbf{M} = \mathbf{T}_{out,N}\mathbf{\Phi'}_N\mathbf{\Gamma}_N\mathbf{\Phi}_N\mathbf{\Phi'}_{N-1}\mathbf{\Gamma}_{N-1}\mathbf{\Phi}_{N-1}\mathrm{L} \quad \mathbf{\Phi}'_2\mathbf{\Gamma}_2\mathbf{\Phi}_2\mathbf{\Phi'}_1\mathbf{\Gamma}_1\mathbf{\Phi}_1\mathbf{T}_{1,in}. \tag{9}$$

where $\mathbf{T}_{1,in}$, $\mathbf{T}_{out,N}$ are transmittance matrices, $\mathbf{\Phi}_i$, $\mathbf{\Phi}'_i$ are the transformation matrices of layer i and $\mathbf{\Gamma}_i$ is the propagation matrix. Transmittance matrices $\mathbf{T}_{i,in}$, $\mathbf{T}_{out,i}$ are shown as

$$\mathbf{T}_{out,i} = \begin{pmatrix} t_{p\ out,N} & 0 \\ 0 & t_{s\ out,N} \end{pmatrix} \tag{10}$$

$$\mathbf{T}_{i,in} = \begin{pmatrix} t_{p1,in} & 0 \\ 0 & t_{s1,in} \end{pmatrix} \tag{11}$$

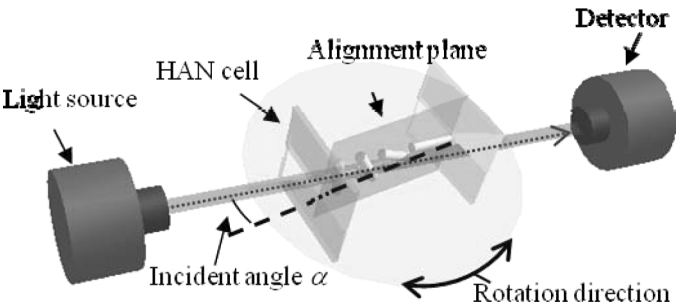

Figure 11. Experimental set-up for new measurement method which measures the angular characteristics in the direction perpendicular to the rubbing direction of HAN cell.

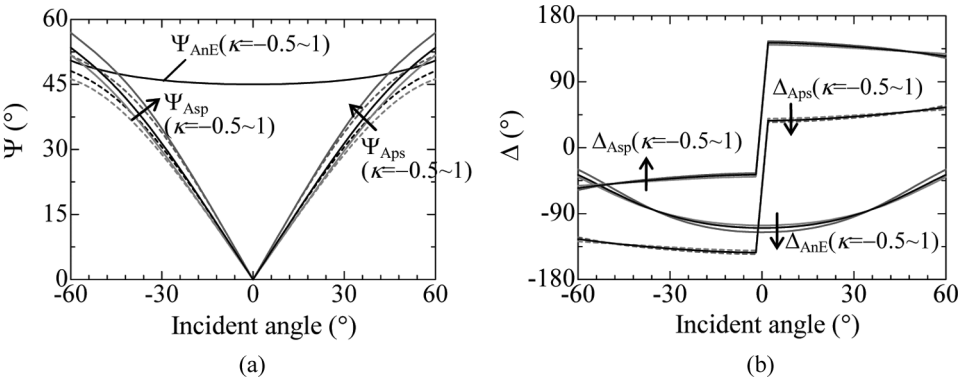

Figure 12. Calculated result of incident angle dependence of the amplitude ratios and the phase differences the HAN cell listed in Table 2. (a) Amplitude ratio Ψ and (b) Phase difference Δ.

where t_p, t_s represent the Fresnel transmission coefficient as shown in the following expressions.

$$t_{pi,j} = \frac{2n_i \cos\theta_i}{n_i \cos\theta_j + n_j \cos\theta_i} \tag{12}$$

$$t_{si,j} = \frac{2n_i \cos\theta_i}{n_i \cos\theta_i + n_j \cos\theta_j}. \tag{13}$$

Propagation matrix $\mathbf{\Gamma}_i$ is shown as

$$\mathbf{\Gamma}_i = \begin{pmatrix} e^{-i\Gamma_i} & 0 \\ 0 & 1 \end{pmatrix} \tag{14}$$

where $\mathbf{\Gamma}_i$ represent the phase difference between ordinary light and extraordinary light.

Transformation matrices $\mathbf{\Phi}_i$, $\mathbf{\Phi}_i'$ are the matrix which rotate P polarized component and S polarized component of light toward ordinary and extraordinary direction, and the matrix which return these, and shown as

$$\mathbf{\Phi}_i = \begin{pmatrix} \cos\Psi & \sin\Psi \\ -\sin\Psi & \cos\Psi \end{pmatrix} \tag{15}$$

$$\mathbf{\Phi}_i' = \begin{pmatrix} \cos\Psi & -\sin\Psi \\ \sin\Psi & \cos\Psi \end{pmatrix} \tag{16}$$

Figure 12 shows the angular characteristics of the amplitude ratios and phase differences of the LC cell listed in Table 2. This figure shows that the angular characteristics of the amplitude ratios and phase differences become different between the several LC cells and these parameters can distinguish the LC parameters including the elastic constant ratio κ.

According to these results, we measured the elastic constant ratio κ, polar anchoring strength of vertical alignment layer B_d and parallel alignment layer B_0. We used liquid crystal of MLC-2038 (Merck Ltd.), vertical alignment layer of RN1765 (Nissan Chemical Industries, Ltd) and parallel alignment layer of SE7992

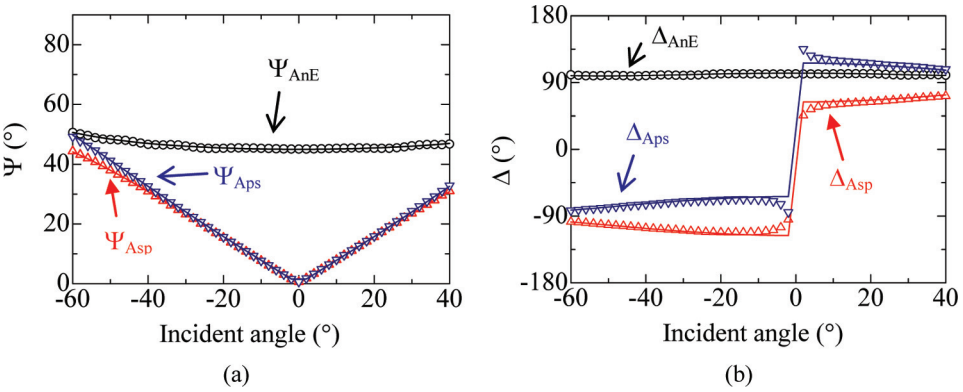

Figure 13. The fitting result between measured and calculated values. (a) Amplitude ratio Ψ; (b) Phase difference Δ.

(Nissan Chemical Industries, Ltd) and fabricated several LC cells with different gaps. We used the same LC material and alignment layer materials, therefore, κ, B_0 and B_d should be constant to the change of cell gap. The fitting result is shown in Figure 13. These figures show that good agreement is obtained between measured and calculated values in both amplitude ratio and phase difference. The experimental results for various cells are shown in Figures 14–16, respectively. The pretilt angle changes with a change of cell thickness (see Fig. 14), though, the measured value are constant to the cell thickness, and are $\kappa = -0.10$, $B_0/k_{11} = 9 \times 10^7$ and $B_d/k_{11} = 8.9 \times 10^7$ and we confirmed validity of our measurement method.

4. Optical Design of the OCB-mode LCD

For the purpose of improving the optical performance of OCB-mode LCD, the optical compensation by using the PDM compensation film is indispensable. Therefore, the evaluation of the alignment distribution of the PDM compensation film and the bend alignment LC cell has become important. However, the quantitative

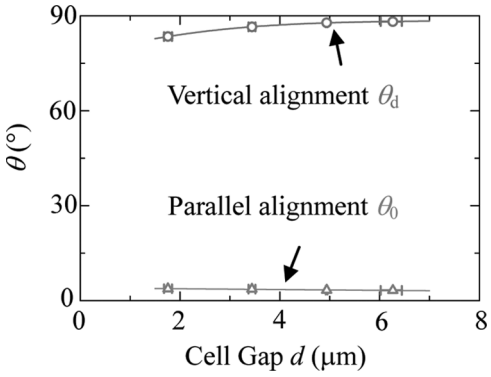

Figure 14. Measured result of cell thickness dependence of the pretilt angle θ_0 and θ_d.

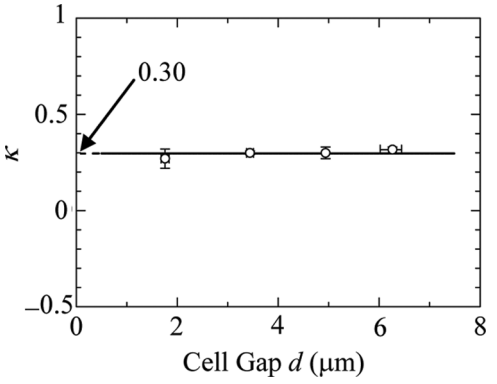

Figure 15. Measured result of cell thickness dependence of the elastic constant ratio κ.

evaluation of LC layer has not been achieved due to the difficulty of the measurement of device parameters of LC cell.

In this section, we measured the alignment distribution of the PDM layer according to the above mentioned measurement method and optimized the bend alignment LC cell. We prepared a sample of PDM compensation film composed of the PDM layer and the biaxial substrate and measured a viewing angle dependence of amplitude ratio Ψ and phase difference Δ. The experiment set-up for the measurement of alignment distribution of PDM compensation film is shown in Figure 17. We used a spectroscopic ellipsometer M-2000 (J. A. Woollam Co., Inc.) for this measurement. The numerical fitting result is shown in Figure 18(a) and (b), respectively. The dotted line is a measure result and the solid line is a calculation result. These figures show that theoretical values and experimental values are fit well. As a result, we successfully obtained the alignment distribution of PDM layer and refractive indices of the biaxial substrate. This result showed that this PDM layer has a hybrid alignment distribution as shown in Figure 19. Figure 20 shows the VT-curve and incident angle property of bend alignment cell. The simulated result shows a good agreement with measure results, and the quantitative

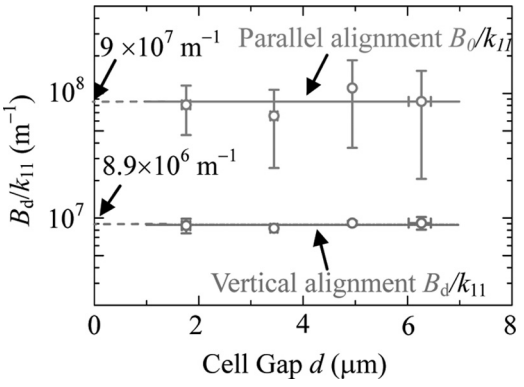

Figure 16. Measured result of cell thickness dependence of the polar anchoring strength of parallel alignment B_0/k_{11} and vertical alignment B_d/k_{11}.

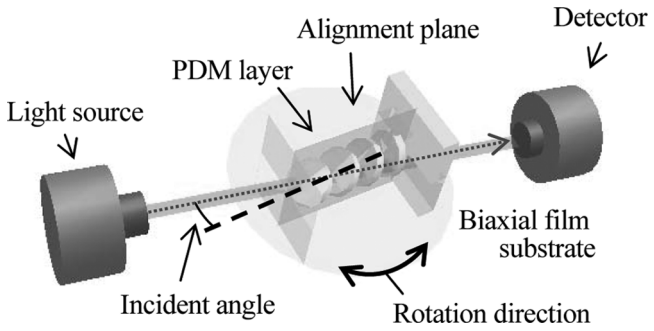

Figure 17. Experimental set-up for measurement of alignment distribution of PDM layer.

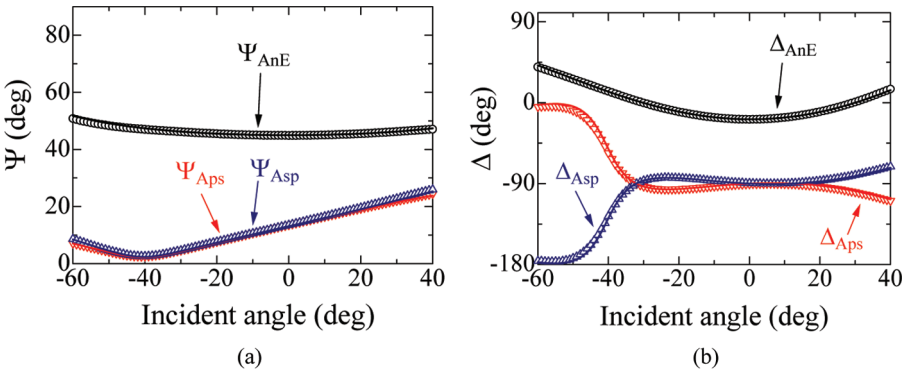

Figure 18. Numerical fitting results to the measurement value of Ψ and Δ. (a) Amplitude ratio Ψ; (b) Phase difference Δ.

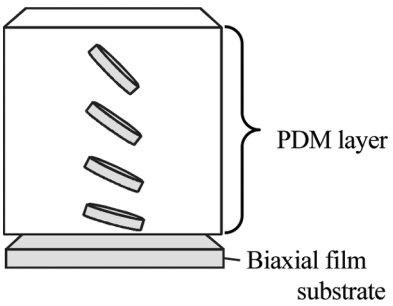

Figure 19. Schematic of measurement result of alignment distribution of PDM layer.

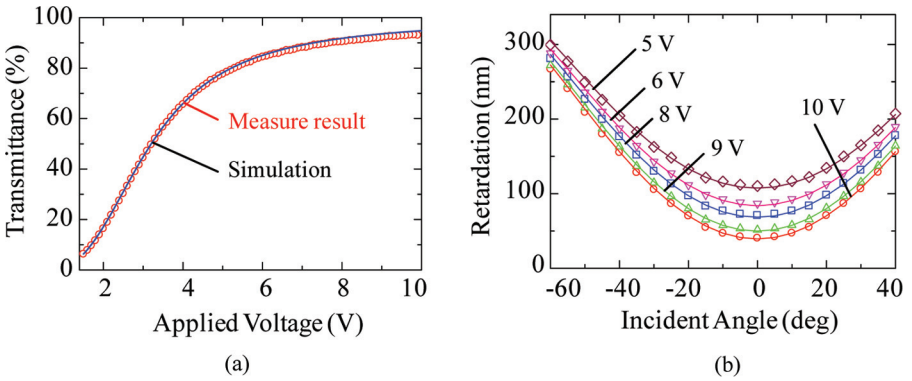

Figure 20. Comparison of the optical property of the Bend-cell between the measured and the calculated results. (a) Voltage - Transmittance curves of Bend-cell; (b) Incident angle - Phase retardation curves of the Bend-cell.

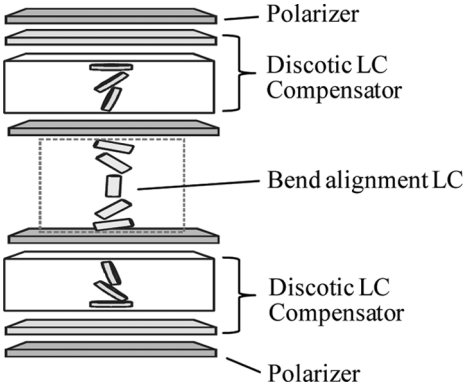

Figure 21. Configuration of the OCB-mode LCD.

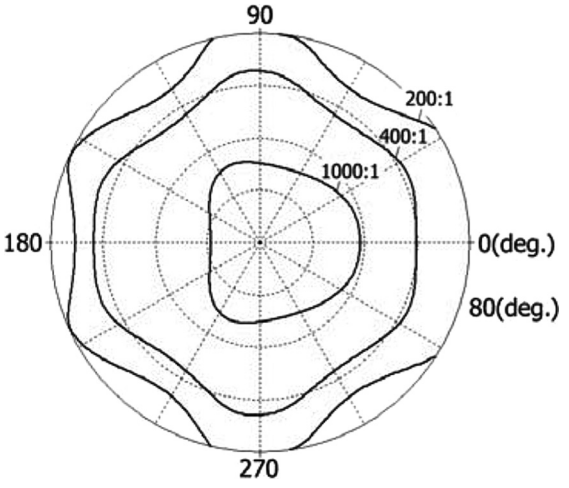

Figure 22. Iso-contrast contour of OCB-mode LCD.

Figure 23. The prototype of 6.5 inch Full-HD field sequential color OCB-mode LCD.

evaluation of LC devices is established by the accurate measurement of LC parameters.

According to the above mentioned measurement results, we optimized the design condition of the OCB mode LCD. Figure 21 shows the configuration of our OCB mode LCD. Our OCB mode LCD is composed of a Bend alignment liquid crystal cell and Discotic LC compensators. Figure 22 shows calculated result of Iso-contrast contour of our OCB mode LC cell. The Δn of LC material is 0.2, cell gap is 3.5 μm and pretilt angle is 8.5 deg. It is seen from this figure that a high contrast ratio is obtained in a wide viewing-angle range.

We fabricated prototype 6.5-inch FSC-OCB mode LCD using our new OCB mode LC cell and scanning LED backlight. We confirmed that our OCB mode LC cell has a high contrast ratio of 1000:1, wide viewing angle over 170 deg (contrast ratio >10:1) and no gray scale inversion in wide viewing-angle range. An additional feature of this FSC-OCB mode LCD is application of an overdrive to suppress the color-shift on FSC-LCDs. Figure 23 shows a photograph of our FSC-OCB mode LCD. We confirmed that high quality FSC-LCD with extremely high contrast ratio in wide viewing angle range, high brightness, and high moving image quality without color break-up is realized.

5. Conclusion

We devised a highly accurate measurement method for the refractive indices of LC materials and the cell thickness using a new extended Jones matrix method considering the multiple reflections and multiple interferences. In addition, we devised a new simple measurement method for the alignment distribution and the surface polar anchoring strength of the parallel and vertical layers using a hybrid alignment liquid crystal cell. We successfully obtained these parameters from the numerical fitting between the measured and the theoretical values of the angle dependency of the phase difference and the amplitude ratio.

Based on these results, we established an evaluation method for a polymerized discotic material compensation film, and clarified the alignment distribution of PDM layer. This evaluation method achieved an accurate control of alignment distribution of PDM layer, and we clarified the optimum conditions for a bend

alignment LC cell and liquid crystal materials. As a result, we successfully obtained OCB mode LCD with high contrast ratio and wide–viewing angle. We developed a new field sequential color OCB mode TFT-LCD with high contrast ratio of 1000:1, wide viewing angle over 170 deg, high quality moving-image capability without color break-up and low power consumption. We confirmed that the accurate evaluation of device parameters of LC can realize the high performance LCD and this FSC-LCD is promising as a display for future high quality moving-image applications.

References

[1] Yamaguchi, Y., Miyashita, T., & Uchida, T. (1993). *SID Symp. Dig. Tech. Papers*, 277.
[2] Wako, K., Yaginuma, H., Kishimoto, T., Ishinabe, T., Miyashita, T., & Uchida, T. (2005). *SID Symp. Digest Tech. Papers*, 666–669.
[3] Mori, H. & Bos, P. J. (1999). *Jpn. Appl. Phys.*, *38*, 2838.
[4] Ito, Y., Matsubara, R., Nakamura, R., Nagai, M., Nakamura, S., Mori, H., & Mihayashi, K. (2005). *SID Symp Digest Tech. Papers*, 986.
[5] Tanaka, N., Kimura, M., & Akahane, T. (2002). *Jpn. J. Appl. Phys.*, *41*, L1502.
[6] Tanaka, N., Kimura, M., & Akahane, T. (2003). *Jpn. J. Appl. Phys.*, *42*, 486.
[7] Jones, R. C. (1941). *J. Opt. Soc. Am.*, *31*, 488.
[8] Yeh, P. (1982). *J. Opt. Soc. Am.*, *72*, 507.
[9] Berreman, D. W. (1972). *J. Opt. Soc. Am.*, *62*, 502.
[10] Yokoyama, H. (1985). *J. Appl. Phys.*, *57*, 4520.
[11] Hung, L. T. & Akahane, T. *et al*. (2004). *Jpn. J. Appl. Phys.*, *43*, L649.
[12] Watanabe, J., *et al*. (2003). *IDW 03 Digest*, 1653.
[13] Kaneko, W., *et al*. (2004). *IDW 04 Digest*, 43.
[14] Hung, L.T., Kimura, M., & Akahane, T. (2005). *Jpn. J. Appl. Phys.*, *44*, 932.
[15] Kimura, M. (2005). Akahane: "KOUGAKU", 34, 244.
[16] Warenghtm, M. & Peralta, S. (2002). *Mol. Cryst. Liq. Cryst.*, *375*, 553.
[17] Okutani, S., Kimura, M., Toriumi, H., Akao, K., Tadokoro, T., & Akahane, T. (2001). *Jpn. J. Appl. Phys.*, *40*, 3288.
[18] Rapini, A. & Paoular, M. (1969). *J. Phys. (Paris), Colloq.*, *30*, C-4.